PHYSICAL REVIEW B **82**, 041310(R) (2010)

Excitation spectra of terahertz Bloch emission in semiconductor superlattices

J. R. Cárdenas,[1] T. Ihara,[2] R. Ferreira,[1] K. Hirakawa,[2] and G. Bastard[1]

[1]*Laboratoire Pierre Aigrain, Ecole Normale Supérieure, CNRS (UMR 8551), Université P. et M. Curie, Université D. Diderot, 24 rue Lhomond, 75005 Paris, France*

[2]*Institute of Industrial Science and INQIE, University of Tokyo, 153-8505 Tokyo, Japan*

(Received 19 April 2010; revised manuscript received 3 June 2010; published 28 July 2010)

We present theoretical and experimental studies of the amplitude of the terahertz (THz) light emitted by biased superlattices excited by fast optical pulses as a function of the pump photon energy. The comparison of the measured transient signal and of its dependence upon the excitation photon energy with a model calculation allows a clear separation between the contributions of the dissociated carriers and bound pairs to the emitted THz field.

DOI: 10.1103/PhysRevB.82.041310 PACS number(s): 78.67.Pt, 78.47.jh

The potential of charge oscillations in semiconductor superlattices as a source of terahertz (THz) radiation has been pointed out a few decades ago.[1] The basic phenomenon, known as Bloch oscillations, is that one electron moving in a periodic potential performs oscillations under the influence of a dc electric field.[2,3] In a biased superlattice (BSL), thanks to the existence of long spatial period ($d \approx 10$ nm), the Bloch oscillation frequency $\omega_B = eFd/\hbar$ corresponds to the THz range of the electromagnetic spectrum. The quantum description of the Bloch oscillations is done in terms of the Wannier-Stark (WS) ladders,[4] whose existence has already been proved experimentally.[5] Besides, key experiments have shown transient Bloch oscillations[6–10] and resonant terahertz photoconductivity.[11] On the theoretical side, Ktitorov *et al.*[12] developed a semiclassical treatment of the frequency dependence of the Bloch oscillations. They found that the dynamical conductivity is negative below ω_B and positive above it, expressing a possible Bloch gain, a conclusion that persists in more elaborate treatments.[13] Terahertz absorption in waveguides loaded with InAs/AlSb supersuperlattice mesas has revealed a frequency-dependent crossover from loss to gain that is related to the Stark ladder.[14]

To observe Bloch oscillations, charges have to be injected in the structure. This can be done either electrically or optically. The former is very involved because of the formation of domains. Great care has to be exercised to diminish their effect.[14] The latter is free from such a drawback since it operates through the interband excitation of an intrinsic BSL. However, optical injection brings about specific effects on the carrier dynamics, such as the presence of excitonic coupling. On the theoretical sides different approaches have been employed to describe the current in a BSL under transient optical excitation and the THz emission associated with the transient current.[15–17] The excitonic coupling may considerably affect the frequency and amplitude of the emitted THz radiation. We shall propose an alternative three-dimensional (3D) modeling to reference[17] that accounts for excitonic effects and describe the interplay between the emissions of the dissociated and bound electron-hole pairs.

In this work, we present a detailed theoretical and experimental study of the dependence of the amplitude of the optically induced THz oscillations in a BSL versus the excitation energy. To this end, we develop a description of excitonic states which, even though less accurate than results from a full numerical diagonalization, nevertheless incorporates the essential of the physics underlying the induced current in BSLs. The small loss of accuracy is advantageously replaced by a much larger flexibility, allowing a more direct estimate of the relative roles of the different geometrical and material parameters affecting the photogenerated THz current in the BSL. We obtain a very good agreement between measured and calculated variations in the emitted amplitude with the excitation energy, allowing to disentangle the bound and dissociated excitonic parts in the measured THz signal.

The experiments were performed at low temperature (5 K) on an undoped superlattice: a GaAs (7.5 nm)/AlAs (0.5 nm) sample with 59 periods. The calculated miniband widths for the conduction and valence bands are: $\Delta_c = 53.3$ meV and $\Delta_v = 4.3$ meV, respectively. Interband excitation was done at fixed bias (12 kV/cm) by optical pulses (temporal width $2\tau_L \approx 100$ fs) delivered by a Ti:sapphire laser. The central photon energy of the pulse was varied around the energy of the main exciton peak at fixed bias but restricted to states related only to WS levels from the first valence and conduction minibands. Transient THz wave forms emitted from the sample were measured using a ZnTe electro-optic detector with a flat sensitivity up to 3.5 THz. Figure 1 shows the time evolution of the THz electric field measured at different laser excitation energies. As a measure of the THz emission amplitude, we plot as symbols in Fig. 2 the difference in signal between the second and third extremas (this choice is discussed below). We discuss in the following this important dependence versus the excitation energy. To this end, we consider the nonstationary wave packets generated by the light pulse.

Before excitation, the sample is in its fundamental state $|0\rangle$ (of energy $\hbar\omega_0$), with all electrons in the valence band. The light couples $|0\rangle$ to the excited states $|n\rangle$ (of energy $\hbar\omega_n$), obtained when one electron is promoted from the topmost valence subband to the lowest conduction subband (see below). We write the time-dependent states of the excited BSL as a linear superposition $|\Psi(t)\rangle = |\Psi_0(t)\rangle + |\Psi_{excit}(t)\rangle = C_0(t)|0\rangle e^{-i\omega_0 t} + \Sigma_n C_n(t)|n\rangle e^{-i\omega_n t}$. The optically induced charge current is related to the mean value of the current operator: $\langle \hat{j}_z(t)\rangle = -e\langle \hat{p}_z\rangle / m_0$ with m_0 and e the bare electron mass and absolute charge, respectively, and $\hat{p}_z$

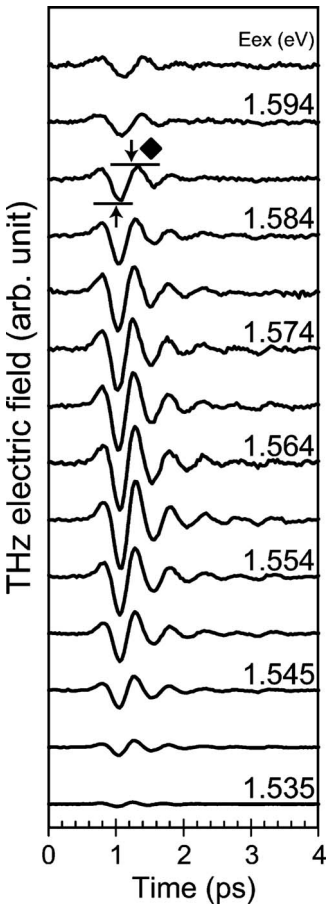

FIG. 1. The transient THz radiation emitted by a GaAs (7.5 nm)/AlAs (0.5 nm) superlattice recorded for various central photon energies of the excitation laser.

the linear momentum operator. Different terms appear in the expression of $\langle \hat{j}_z(t) \rangle$. The THz current comes from those proportional to $C_n^*(t)C_{n'}(t)\exp\{i[\omega_n - \omega_{n'}]t\}$, and is thus inherent solely to the excited states.

Before discussing the optically induced THz quantum mechanical current, it is worth noticing that it has two characteristics not in agreement with the well-known Bloch oscillation (characterized by a single angular frequency ω_B) predicted by the one-carrier one-band semiclassical model.[18] First, its time evolution at early times is not an intrinsic property of a BSL but depends on the excitation details incorporated in the time-dependent dipolar coupling terms. However, for times longer than τ_L, but that can be short compared to the THz oscillations period (see Fig. 1), the coefficients assume their asymptotic form $C_n(\infty)$, and the carriers dynamics is no longer excitation driven. Second, it is *a priori* not a monochromatic oscillation, since it results from interferences involving all excited states, with different beating frequencies $\omega_n - \omega_{n'}$. As shown below, and also pointed out in the literature,[6,8–10,17] this is due to the photogeneration of excitons by the interband pulse, both in dissociated and in bound orbits (for the electron-hole relative motion), each set of states giving a separate contribution to the THz emission. In this work we give explicit expressions for these currents. To this end, we use standard lowest-order

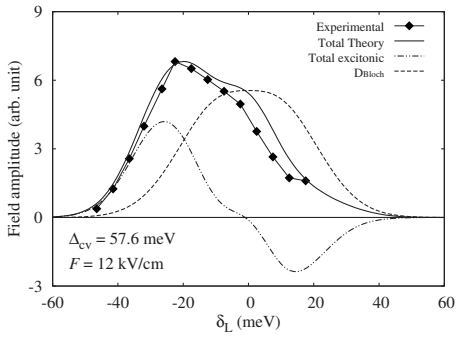

FIG. 2. Symbols: amplitude of the emitted THz electric field (as defined by the second-to-third extremas amplitude difference) versus detuning δ_L in the GaAs (7.5 nm)/AlAs (0.5 nm) superlattice. The amplitude of the time derivative of the total current $j_{Bloch}(t)+j_{1S}(t)$ is plotted in the same figure as a solid line. The dashed line is the band-to-band contribution and the dashed-dotted line is the total excitonic contribution.

perturbation (a good approximation in the weak excitation case considered in this work) to evaluate $C_n(\infty)$ and obtain,

$$\langle \hat{j}_z(t) \rangle \to a_0 I_L \sum_{n,m} A_{m,n} \sin(\omega_{mn}) \quad t \gg \tau_L,$$

$$A_{m,n} = \hat{V}_{0,n}(i\hat{p}_z)_{n,m}\hat{V}_{m,0}e^{-(\omega_{mn}\tau_L/2)^2}e^{-\{[\bar{\omega}_{mn}-(\omega_0-\omega_L)]\tau_L\}^2}, \quad (1)$$

where $\hat{V}_{0,n}$ is the matrix element for the interband light excitation (its squared modulus is the oscillator strength for the $|0\rangle \to |n\rangle$ transition), $\omega_{mn}=\omega_n-\omega_m$, $\bar{\omega}_{mn}=(\omega_n+\omega_m)/2$, a_0 is a material-dependent constant and we assumed a Gaussian pulse with electric field amplitude $E(t)=\tilde{E}(0)e^{-t^2/2\tau_L^2}e^{-i\omega_L t}+\text{c.c.}$ and $I_L=|\tilde{E}(0)|^2$. The current is thus given by a sum of sinusoidal terms, involving the different excited states that can be optically reached from the ground one. Finally, the emitted THz field is related to the time derivative of the current and its amplitude is associated with the quantities $D_{n,m}=\omega_{mn}A_{m,n}$.

To proceed further, we need to specify the states $|n\rangle$. Following Yang *et al.*,[17] we consider only the more bound $|X_{1S}\rangle$ and the dissociated $|X_c\rangle$ excitonic states. The latter are approximated by independent electron-hole states whereas the former are evaluated in two steps, as follows. First, we use a variational procedure with Gaussian trials for the in-plane relative motion to obtain separately the 1*S*-like states associated with each electron-hole interband transition. Then, the Coulombic coupling is diagonalized within the basis generated by the previous decoupled excitons. This last step generates truly 3D bound states and provides better energies and oscillator strengths for the transitions, in particular, those with important strengths [which dominate both the interband photogeneration of electron-hole pairs and the amplitude of the intraband charge oscillations; see Eq. (1)]. From the two sets of states, one obtains three contributions to the current: intracontinuum, intrabound, and mixed terms involving both bound and dissociated states. We checked that for the structures considered in this work, the last contribution is considerably smaller than the two others.

After summation over the in-plane relative motion and z-dependent degrees of freedom, we obtain that the continuum contribution for $t \gg \tau_L$ writes,

$$j_{Bloch}(t) = A_B \sin(\omega_B t),$$

$$A_B = A_0 e^{-(\omega_B \tau_L/2)^2} \int_{-\infty}^{\infty} \frac{d\tau}{\tau} \exp\left[-\left(\frac{\tau}{2\tau_L}\right)^2\right] \cos\left(\frac{\delta_L}{\hbar}\tau\right) \times J_1\left[2Z_{cv} \sin\left(\frac{\omega_B \tau}{2}\right)\right], \quad (2)$$

where J_1 is the Bessel function of the first kind, $\delta_L = \hbar\omega_L - E_G$ is the laser detuning ($\delta_L = 0$ corresponds to the central excitation of the conduction and valence Wannier-Stark ladders), $Z_{cv} = -(\Delta_c + \Delta_v)/2eFd$, and A_0 a material constant expressible in terms of a_0. Figure 2 shows the variation in the quantity $D_{Bloch} = \omega_B A_B$ versus the excitation detuning δ_L (dashed line). We see that the amplitude of the Bloch oscillation displays a symmetrical curve as a function of δ_L with a maximum current and acceleration amplitudes for resonant excitation at the central Wannier-Stark interband transition. Note that this strikingly contrasts with the carrier photoexcitation (electron/hole population after pulse passage) which increases continuously to eventually saturate at large $\hbar\omega_L$.

The current through the discrete sequence of bound levels is a sum of terms, each involving two states: $j_{1S}(t) = \Sigma_{l,l'} j^{1S}_{l,l'}(t)$, where $j^{1S}_{l,l'} = A_{l,l'} \sin[\Omega_{l,l'} t]$ with $\hbar\Omega_{l,l'} = E^{1S}_l - E^{1S}_{l'}$ their energy separation and $A_{l,l'}$ evaluated according to the general formula [Eq. (1)]. The emitted THz field is related to the time derivative of the current and thus associated to the quantities $D_{l,l'} = \Omega_{l,l'} A_{l,l'}$. Each $D_{l,l'}$ component has a maximum contribution when the central excitation energy coincides with $\bar{\omega}_{ll'}$ [see Eq. (1)]. We have numerically calculated the time derivative of the total $1S$ current $j_{1S}(t)$ and plotted in Fig. 2 the difference in signal between the second and third extrema, as a function of the excitation detuning (dashed-double-dotted line). One obtains an almost antisymmetrical curve around $\delta_L = 0$. On the contrary the unbound states amplitude does not change sign, evidencing the importance of the 3D nature of the band-to-band transitions. Note that our finding contradicts the results of early models[19] where the carrier in-plane motions were disregarded (by considering BSL structures as one-dimensional systems), leading to the prediction of breathing modes for the excitation of independent carriers in coupled quantum wells and BSLs.

As mentioned previously, we consider the difference in signal between the second and third extremas of the measured THz field. This choice allows a better access to the amplitude of the intrinsic time oscillations of a BSL by getting rid of two undesired effects (not discussed in this work): (i) the pulse induced time variation in the current at short times ($t \leq \tau_L$; see above) and (ii) the amplitude decay observed at longer times and due to dephasing mechanisms. In order to interpret the experiments, we have numerically evaluated the time derivative of the total current $j_{Bloch}(t) + j_{1S}(t)$ and plotted with a bold line in the same Fig. 2 its second-to-third extremas amplitude difference. Note

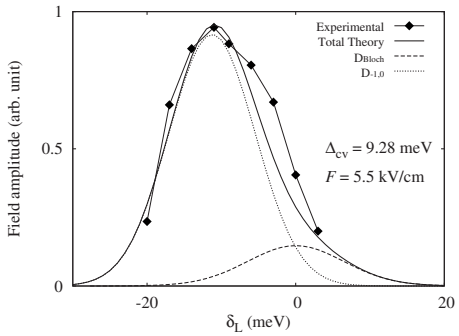

FIG. 3. Symbols: amplitude of the emitted THz electric field (as defined by the second-to-third extremas amplitude difference) versus detuning δ_L in the 11.8 nm/2.4 nm $GaAs/Al_{0.3}Ga_{0.7}As$ superlattice. The amplitude of the time derivative of the total current $j_{Bloch}(t) + j_{1S}(t)$ is plotted in the same figure as a solid line. The dashed line is the band-to-band contribution and the dotted line is the main excitonic contribution to the $1S$ amplitude.

that in the fitting procedure, the excitonic and band-to-band contributions depend on a single material constant (a_0). Thus, it is meaningful to compare them and to add them to produce the total THz electrical field. We obtain a very good agreement for the amplitude of the optically induced THz signal. Small differences possibly come from damping effects and the finite spectral width of the detection system, both present in practice but not included in the calculations.

The total emission at positive detuning is dominated by the continuum states, that is to say, by independent electrons and holes performing Bloch oscillations, while the excitonic contribution is more important at negative detunings.[17] This explains the asymmetrical line shape of the amplitude versus detuning curve. It is worth recalling that excitons are neutral entities and the existence of a current of excitonic origin can be traced back to the fact that different excitonic states have different electron and hole spatial localization along the growth axis. Thus, the exciton current follows because of the simultaneous excitation of several exciton states between which the current operator is nonvanishing.

Similar experiments (Fig. 3) have been carried out on a 11.8 nm/2.4 nm $GaAs/Al_{0.3}Ga_{0.7}As$ superlattice which displays much smaller bandwidths ($\Delta_c = 8.94$ meV and $\Delta_v = 0.34$ meV) than the one shown in Fig. 2. For this THz measurement, we used excitation laser pulses with a wider temporal width ($2\tau_L \approx 200$ fs) and a thicker electro-optic sensor (~ 700 μm thick), whose bandwidth is 2.5 THz. We have found both experimentally and theoretically that the THz signal is much weaker than in the SL with wide miniband. In addition, in the narrow miniband SL, the excitonic contribution is enhanced over the band to band compared to the situation found in the wide miniband SL. We find a good agreement between the calculated and measured excitation spectra of the THz field. This gives further support to our analysis.

In conclusion, we have considered the THz field emission of two biased superlattices with very different miniband widths and show that the contributions of independent electron/hole pairs and bound excitons to the total charge

oscillations can be very different for different samples. Our modeling, based on the calculation of the time-dependent total wave function of the biased superlattice in the presence of a fast interband optical pulse, provides a very good quantitative description of the intrinsic amplitude of oscillations of the emitted THz field as a function of the optical pulse energy. We have evidenced the crucial importance played by the preparation stage of the Bloch oscillation while it appears that the damping and relaxation effects[20] play a minor part in this preparation stage. Owing to its flexibility, this wave-packet analysis can be easily implemented for other structures and experimental situations.

The LPA-ENS is "UMR8551 du Centre National de la Recherche Scientifique et est associée aux Universités Paris 6 et Paris 7." J.R.C. has been supported by the program AlBan, the European Union Programme of High Level Scholarships for Latin America, Scholarship No. E07D402676BR. This work has been supported by a CNRS/JSPS International Collaboration Programme, the Grant-in-Aid from JSPS (Grant No. 22241036), ANR project ROOTS and by a Special Coordination Fund for Promoting Science and Technology from MEXT (NanoQuine). One of us (G.B.) gratefully acknowledges JSPS for support (International Exchange Programme).

[1] L. Esaki and R. Tsu, IBM J. Res. Dev. **14**, 61 (1970).
[2] F. Bloch, Z. Phys. **52**, 555 (1929).
[3] C. Zener, Proc. R. Soc. London, Ser. A **145**, 523 (1934).
[4] G. H. Wannier, Rev. Mod. Phys. **34**, 645 (1962).
[5] E. E. Mendez, F. Agullo-Rueda, and J. M. Hong, Phys. Rev. Lett. **60**, 2426 (1988).
[6] C. Waschke, H. G. Roskos, R. Schwedler, K. Leo, H. Kurz, and K. Köhler, Phys. Rev. Lett. **70**, 3319 (1993).
[7] T. Dekorsy, P. Leisching, K. Köhler, and H. Kurz, Phys. Rev. B **50**, 8106 (1994).
[8] J. Feldmann, K. Leo, J. Shah, D. A. B. Miller, J. E. Cunningham, T. Meier, G. von Plessen, A. Schulze, P. Thomas, and S. Schmitt-Rink, Phys. Rev. B **46**, 7252 (1992).
[9] K. Leo, P. H. Bolivar, F. Bruggemann, R. Schwedler, and K. Kohler, Solid State Commun. **84**, 943 (1992).
[10] N. Sekine and K. Hirakawa, Phys. Rev. Lett. **94**, 057408 (2005).
[11] K. Unterrainer, B. J. Keay, M. C. Wanke, S. J. Allen, D. Leonard, G. Medeiros-Ribeiro, U. Bhattacharya, and M. J. W. Rodwell, Phys. Rev. Lett. **76**, 2973 (1996).
[12] S. A. Ktitorov, G. S. Simin, and V. Y. Sindalovskii, Sov. Phys. Solid State **13**, 1872 (1972).
[13] H. Willenberg, G. H. Döhler, and J. Faist, Phys. Rev. B **67**, 085315 (2003).
[14] P. G. Savvidis, B. Kolasa, G. Lee, and S. J. Allen, Phys. Rev. Lett. **92**, 196802 (2004).
[15] T. Meier, F. Rossi, P. Thomas, and S. W. Koch, Phys. Rev. Lett. **75**, 2558 (1995).
[16] J. Hader, T. Meier, S. W. Koch, F. Rossi, and N. Linder, Phys. Rev. B **55**, 13799 (1997).
[17] L. Yang, B. Rosam, J.-M. Lachaine, K. Leo, and M. M. Dignam, Phys. Rev. B **69**, 165310 (2004).
[18] K. Leo, *High Field Transport in Semiconductor Superlattices*, Springer Tracts in Modern Physics Vol. 187 (Springer, Berlin, 2003).
[19] A. M. Bouchard and M. Luban, Phys. Rev. B **52**, 5105 (1995).
[20] R. Ferreira, T. Unama, K. Hirakawa, and G. Bastard, Appl. Phys. Express **2**, 062101 (2009).